LETTER

doi:10.1038/nature15753

North Pacific deglacial hypoxic events linked to abrupt ocean warming

S. K. Praetorius[1]†, A. C. Mix[1], M. H. Walczak[1], M. D. Wolhowe[1], J. A. Addison[2] & F. G. Prahl[1]

Marine sediments from the North Pacific document two episodes of expansion and strengthening of the subsurface oxygen minimum zone (OMZ) accompanied by seafloor hypoxia during the last deglacial transition[1–4]. The mechanisms driving this hypoxia remain under debate[1–11]. We present a new high-resolution alkenone palaeotemperature reconstruction from the Gulf of Alaska that reveals two abrupt warming events of 4–5 degrees Celsius at the onset of the Bølling and Holocene intervals that coincide with sudden shifts to hypoxia at intermediate depths. The presence of diatomaceous laminations and hypoxia-tolerant benthic foraminiferal species, peaks in redox-sensitive trace metals[12,13], and enhanced $^{15}N/^{14}N$ ratio of organic matter[13], collectively suggest association with high export production. A decrease in $^{18}O/^{16}O$ values of benthic foraminifera accompanying the most severe deoxygenation event indicates subsurface warming of up to about 2 degrees Celsius. We infer that abrupt warming triggered expansion of the North Pacific OMZ through reduced oxygen solubility and increased marine productivity via physiological effects; following initiation of hypoxia, remobilization of iron from hypoxic sediments could have provided a positive feedback on ocean deoxygenation through increased nutrient utilization and carbon export. Such a biogeochemical amplification process implies high sensitivity of OMZ expansion to warming.

Models suggest enhanced ocean deoxygenation in response to future global warming, owing to both a reduction in oxygen solubility and decreased subsurface ventilation related to thermal stratification[14,15]. Uncertainty in these projections reflects weak constraints on the response of marine primary productivity to warming[16] and the extent to which ecosystem changes will translate to carbon export and remineralization[17], thus altering subsurface oxygen demand. Once hypoxia is initiated, seafloor biogeochemical cycling may sustain and enhance low-O_2 conditions via a threshold effect[18]. For example, reductive mobilization of sedimentary iron may further stimulate primary productivity in surface waters of high-nitrate-low-chlorophyll (HNLC) regions if it occurs within an ocean depth range susceptible to mixing into the euphotic zone; this in turn would increase oxygen demand in underlying waters, until sulfidic conditions ensue and limit further supplies of dissolved iron from the sediments to the upper water column[19].

Data from intermediate water depth marine sediment cores across the North Pacific (Fig. 1) document expansion and strengthening of the OMZ during the Bølling–Allerød interstade (14.7–12.9 thousand years ago (ka)) and earliest part of the Holocene interglacial (11.5–10.5 ka)[1–4]. Mechanisms proposed to account for deglacial hypoxia include a decrease in ocean ventilation related to changes in ocean circulation[3,5], and increased oxygen demand related to enhanced export productivity[6–11].

So far, no consistent evidence links decreased ventilation rate with these hypoxic events. Benthic-planktonic radiocarbon age differences on the Gulf of Alaska margin show no significant deviation from the long-term mean (725 ± 200 yr) during either of the hypoxic events (Fig. 2), and when benthic-planktonic increases do occur (during the Younger Dryas interval; 12.9–11.7 ka), they are not associated with hypoxia[20].

Mechanisms to stimulate productivity over such widespread oceanographic settings remain unclear. However, once hypoxia is initiated in a subsurface water mass, it may spread over a greater area than the region of elevated productivity[6], because downward mixing of oxygen beyond the range of shallow wind-driven mixing is small. Iron release from continental shelves in response to sea-level rise has been suggested as a potential driver of increased productivity in HNLC regions such as the subpolar North Pacific[1,2]. However, regional sea-level histories differ owing to isostatic responses to ice unloading. For the sea-level mechanism to work, long-distance transport of iron would be required.

Alternative hypothetical mechanisms to stimulate North Pacific productivity have invoked increased upwelling of macronutrients during hypoxic events[9]. This would require reduced stratification, paradoxically at a time of northern hemisphere warming and enhanced freshwater input to the marginal ocean from melting ice sheets. This mechanism does not account for the fact that macronutrients such

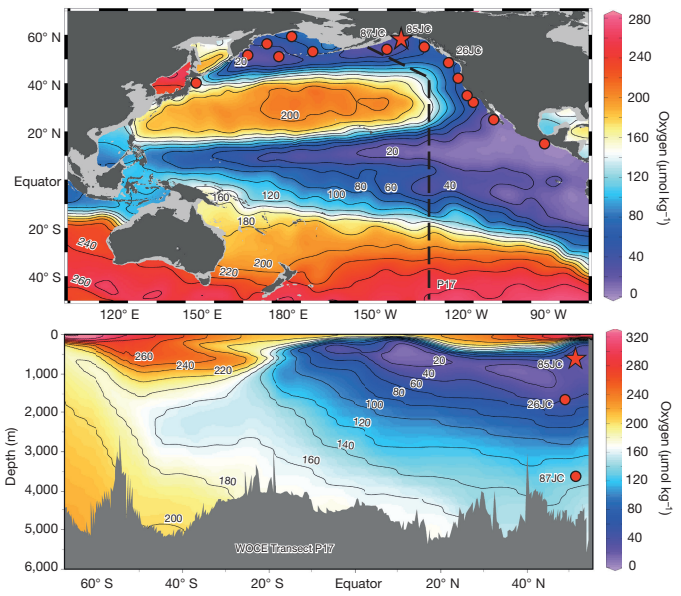

Figure 1 | Study area and core locations. Top, colour shading on map shows modern oxygen concentration at 400 m depth, with the clearly defined OMZ across the North, Eastern, and Equatorial Pacific. The core site EW0408-85JC in this study is indicated with a red star; other core sites that document deglacial hypoxic/productivity events are indicated with red circles[4]. Bottom, meridional cross-section of oxygen concentration in the modern Eastern Pacific, with the location of core sites used in the $\delta^{18}O$ depth transect (Fig. 4). Maps were generated with Ocean Data View[31].

[1]College of Earth, Ocean, and Atmospheric Sciences, Oregon State University, Corvallis, Oregon 97331, USA. [2]US Geological Survey, Menlo Park, California 94025, USA. †Present address: Department of Global Ecology, Carnegie Institution for Science, Stanford, California 94305, USA.

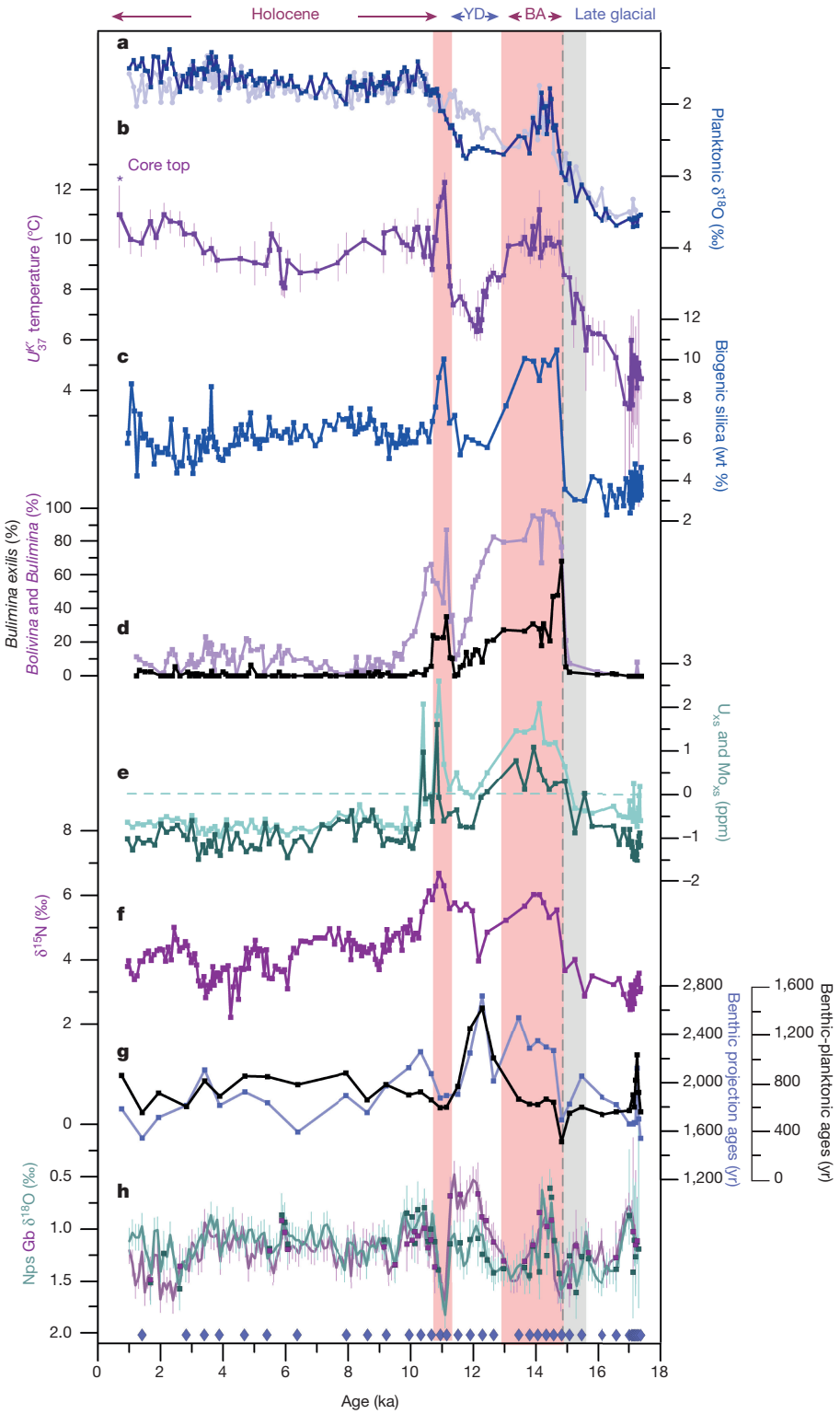

Figure 2 | Data from core EW0408-85JC. a, Planktonic $\delta^{18}O$ data (Nps: dark blue, Gb: light blue)[2]. **b**, Alkenone palaeotemperature (purple) and error estimates (light purple bars). **c**, Biogenic opal percentages relative to bulk sediment (blue)[2]. **d**, Relative abundance of low-oxygen benthic foraminifera (*Bolivina* and *Bulimina* genera: light purple, *Bulimina exilis*: black). **e**, Redox-sensitive trace metal concentrations (Mo is light green, U is dark green) in excess values relative to lithogenic background (dashed line)[12,13]. **f**, Sedimentary $\delta^{15}N$ (dark violet)[13]. **g**, Benthic-planktonic radiocarbon age differences (black) and benthic projection ages calculated with respect to atmospheric $\Delta^{14}C$ (blue)[20]. **h**, Reconstructions of near-surface seawater $\delta^{18}O$ based on the planktonic species Gb (green) and Nps (light violet), with depth-based pairs indicated as square symbols and values linearly interpolated at 100-yr intervals shown as a trend line. Age controls are from Davies-Walczak *et al.*[20] and are indicated with blue diamonds at the bottom of the plot. The pink bars represent the two laminated intervals in core EW0408-85JC, the grey bar indicates the zone in which changes in SST, trace metals, and benthic fauna slightly precede the onset of laminations (dashed grey line) (expanded view in Extended Data Fig. 7). The timing of major climate intervals are indicated at the top of the plot: Holocene (11.6–0 ka), Younger Dryas (YD; 12.9–11.7 ka), Bølling–Allerød (BA; 14.6–12.9 ka), late glacial (18–14.7 ka). Nps, *Neogloboquadrina pachyderma*; Gb, *Globigerina bulloides*.

as phosphate and nitrate, supplied today by vertical mixing, do not limit productivity in the region. Further, most deep mixing occurs in winter, when light is limiting. Although deep upwelling also provides some iron, it is not currently enough to consume the macronutrients; relief of iron limitation in the past would require an additional iron source. Haline stratification due to ice melt may have enhanced marine productivity by reducing deep mixing of plankton out of the euphotic zone[10]. Haline inhibition of deep mixing would, however, reduce the source of subsurface iron[21].

Distinguishing among the various hypotheses requires separating sea-surface temperature (SST) and salinity effects on near-surface stratification and subsurface ventilation. Here we pair a new high-resolution palaeotemperature record based on the $U^{K'}_{37}$ alkenone index from the Gulf of Alaska with benthic faunal assemblages and proxies for ventilation rate, export productivity, and surface stratification to evaluate the sequence of oceanographic changes leading to hypoxia in a marine sediment core located in the upper reaches of the modern OMZ (EW0408-85JC, 59° 33.32′ N, 144° 9.21′ W, 682 m depth). The various proxy indicators are co-registered with little or no impact from chronologic error, because they occur in the same sediment core. We find that two abrupt deglacial warming events of 4–5 °C coincide with increases in nutrient utilization, export productivity, and the sudden onset of hypoxia. Alkenone SST reconstructions from other sites in the North Pacific show similar trends (Extended Data Fig. 9), indicating these were significant regional temperature fluctuations.

Palaeotemperatures in the northern Gulf of Alaska were lowest (~5 °C) near 17.0 ka, (Fig. 2), coincident with a peak in ice-rafted debris (IRD)[2]. Warming commenced near 16.5 ka, before the Bølling interstade in Greenland. Warming then accelerated, with a rapid 3–4 °C rise from 15.2 to 14.7 ka, coincident with the Bølling onset; warm conditions persisted until 13.0 ka.

The high relative abundance of the benthic foraminifera *Epistominella pacifica* during the late glacial period (17–15 ka) indicates that the water column was less oxygenated than modern conditions (Extended Data Fig. 4). Following the accelerated warming into the Bølling, severe hypoxia seems to have started abruptly at 14.7 ka, as documented by a sharp transition to sediment laminations, a shift to benthic populations dominated by the low-oxygen foraminifera *Bulimina exilis*, and an increase in sedimentary molybdenum and uranium concentrations (Fig. 2). This transition coincided with increased concentrations of biogenic silica and marine organic carbon and a rise in the $\delta^{15}N$ of organic matter, reflecting enhanced nutrient utilization and export productivity[2,13] (Extended Data Figs 5 and 6).

The increase in redox-sensitive trace metals (excess Mo and U)[12,13] and low-oxygen benthic species slightly preceded the increase in biogenic silica and total organic carbon (TOC) (by 2–5 cm, about 300 ± 100 yr) during the Bølling–Allerød transition (Extended Data Fig. 7). This implies that local hypoxia may have developed before the increase in export productivity, most likely through a reduction in oxygen solubility related to ocean warming. In the absence of bioturbation, cm-scale depth offsets in these proxies may in part reflect redox gradients in the sediment column. However, a deeper site in the Gulf of Alaska (EW0408-26JC; 1,620 m) shows benthic faunal evidence for a gradual decrease in oxygen, starting with the early warming at 16 ka (Extended Data Fig. 8), well in advance of productivity enhancement.

The benthic faunal assemblages and trace metals indicate that hypoxic conditions persisted while surface palaeotemperatures remained elevated near 10 °C during the Bølling–Allerød interstade. More oxygenated conditions returned only when alkenone palaeotemperatures fell by 4 °C during the Younger Dryas interval (12.9–11.7 ka). Another abrupt 5 °C warming occurred during the transition into the early Holocene (11.4–10.9 ka); SSTs above 11 °C were again accompanied by an increase in biogenic silica concentrations, a rise in $\delta^{15}N$, and a return to hypoxic conditions (evidenced by laminations, low-oxygen benthic fauna, and an increase in authigenic Mo and U concentrations).

Benthic faunal assemblage data document crossing of an ecological threshold during both episodes of hypoxia, with an abrupt transition from virtual absence to dominance of *Bulimina exilis* at the start of each event, indicating that the system switched nearly instantaneously from intermediate to severe hypoxia. Shortly following the initial peaks in *Bulimina exilis*, the site was re-colonized by other low-oxygen *Bolivina* species (Fig. 2), indicating a slight relaxation from extreme to strong hypoxia. *Epistominella pacifica* reappears in the faunal assemblages during the Younger Dryas and early Holocene, consistent with the return of more oxic conditions in bottom waters as the surface ocean cooled (Extended Data Fig. 4). Some low-oxygen benthic fauna and redox-sensitive trace metals persisted after decreases in SST and reduction in biogenic silica, suggesting a lag in the amelioration of hypoxic conditions. A trend of increasing relative percentage of *Uvigerina peregrina* during the Holocene indicates the water column became progressively well oxygenated.

The alkenone palaeotemperature data show that most of the anomalously low $\delta^{18}O$ at onset of the Bølling interstade (1.1‰ of the total 1.5‰ change) reflects warming (Fig. 2). The temperature and ice-volume-corrected seawater $\delta^{18}O$ record is primarily an indicator of freshwater input from land, which is typically high in this stormy and glaciated region. Freshwater input varies near the onset of the Bølling–Allerød interstade hypoxic event, but there are no consistent trends that would indicate a sustained freshening of the surface ocean during either hypoxic event. This finding precludes haline stratification as a primary cause of hypoxia at this location. Accumulation of terrigenous silt is also low during the hypoxic intervals, arguing against glacial runoff and rock flour as a primary source of iron to fertilize high productivity at these times. However, high rates of terrigenous sediment accumulation on the shelf and slope during the late glacial period[2] would have provided a reservoir of iron in the sediments, which may then have been available for release in a bioavailable form upon initiation of hypoxia.

Warming slightly precedes both the increase in productivity and the onset of hypoxia (rates of warming are 0.6–1.2 °C per century in the lead up to both events; Extended Data Fig. 3), making it likely that temperature exerted a primary initial trigger for biogeochemical amplifying effects responsible for extensive hypoxia. This observation narrows the hypotheses to two (Fig. 3): either (1) rapid warming led to modest regional hypoxia via thermal solubility effects, which in turn stimulated marine primary productivity indirectly through the mobilization of iron from hypoxic sediments, or (2) rapid warming directly stimulated marine productivity, which led to higher consumption of oxygen in subsurface waters through remineralization of organic matter, with possible further amplification via reductive iron release. In both hypotheses, warming leads to hypoxia; they are not mutually exclusive. Both suggest increases in nutrient utilization in what is now an iron-limited system; this is supported by rising $\delta^{15}N$ of organic matter[13] (Fig. 2) coupled to an increase in $\delta^{13}C$ in planktonic foraminifera (Extended Data Figs 5 and 6) during the warm events.

The first hypothesis requires warming in subsurface waters. If the $\delta^{18}O$ excursion (−1‰) in the benthic record were due to an increase in temperature alone, it would imply subsurface warming of about 4–5 °C at a depth of 682 m. The presumed implausibility of such warming at depth has led to the interpretation of this feature as a pulse of low salinity waters[2]. However, the occurrence of similar but smaller benthic $\delta^{18}O$ anomalies (−0.4–0.6‰) in deeper sites during the Bølling–Allerød interstade (Fig. 4, Extended Data Fig. 1) is consistent with up to about 2.0 °C abyssal warming; pulses of low salinity are implausible in the deep basin.

Based on known thermal solubility effects, a 2.0 °C warming would reduce subsurface oxygen concentrations by about 17 μmol kg^{-1} (ref. 22), which if initiated relative to the modern OMZ of the North Pacific, would drive the site EW0408-85JC to less than 5 μmol kg^{-1}, enough for significant ecological impacts[23] (Fig. 1). The benthic fauna

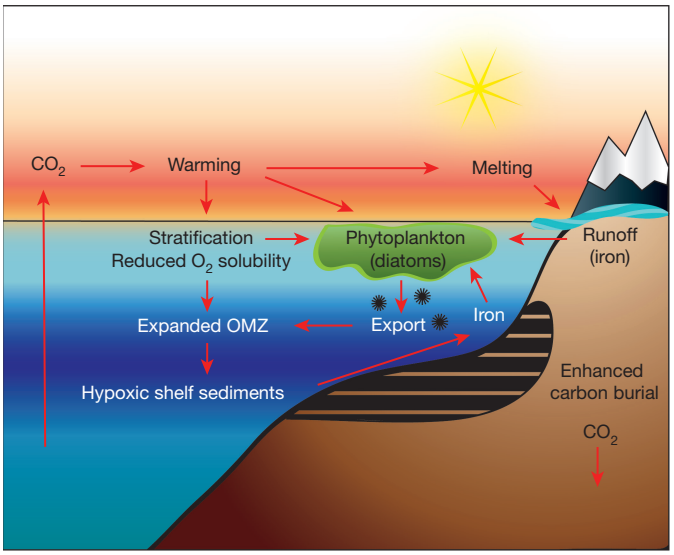

Figure 3 | Schematic diagram of feedback processes linking ocean warming to enhanced export productivity. As CO_2 is vented from the deep ocean throughout the deglaciation, the ocean warms along with the climate. Warming reduces oxygen solubility and promotes stratification, leading to an expansion of the OMZ and a greater area of suboxic sediments in the shallow subsurface, which remobilizes bioavailable iron to fuel marine productivity, further depleting subsurface oxygen concentrations as organic matter is exported and respired at depth. The availability of iron and warm, stratified conditions favours large diatoms[27], which have high export efficiency owing to high settling velocities.

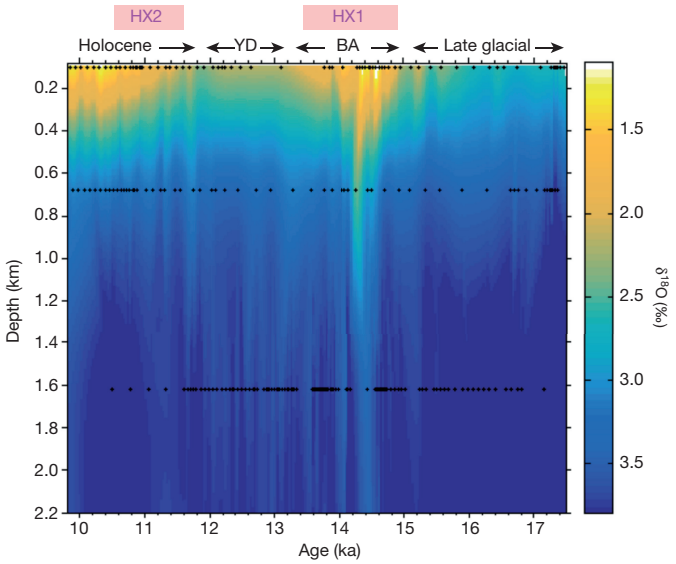

Figure 4 | Deglacial depth transect of $\delta^{18}O$ in the Gulf of Alaska. Planktonic foraminiferal data (Nps $\delta^{18}O$) from core EW0408-85JC is used for the subsurface thermocline (depth = 100 m). Benthic foraminiferal $\delta^{18}O$ data (expressed as *Uvigerina peregrina* equivalent values) from various core sites are plotted at depth: EW0408-85JC (682 m)[2], EW0408-26JC (1,620 m), and EW0408-87JC (3,680 m) (data plotted in Extended Data Fig. 1). The plot is truncated at 2.2 km depth for an expanded view of intermediate depths. All data are corrected for the global isotopic effects of changing ice volume[37]. Labels identify climate intervals specified in Fig. 2. The timing of the deglacial hypoxic events are indicated with pink bars. Details of the age models of individual cores are included in Methods.

suggest slightly lower oxygenation than today before the Bølling–Allerød interstade (Extended Data Fig. 4), so subsurface thermal solubility effects might have been sufficient to trigger local hypoxia and initial vertical expansion of the OMZ, but are unlikely to drive widespread or severe hypoxia. If shoaling of the hypoxic boundary layer was sufficient to trigger an iron and phosphate[24] release from shallow sediments (that is, within reach of mixing into the euphotic zone), an ecological response favouring carbon export would have amplified initial thermally driven hypoxia. Production of larger diatoms enhances carbon export to the subsurface[25], and these diatom species are known to increase in relative abundance in response to increased iron input[26] and stratification[27]. Dominance of large diatoms in the overall species assemblage has been found elsewhere in the Northeast Pacific during deglacial warming[17].

The second hypothesis revives a longstanding debate in biological oceanography following Eppley's inference[28] that warming enhances phytoplankton growth rate directly through a Q_{10} (exponential physiological rate) effect. Such an effect may be important in subpolar regions, and may be enhanced by stratification that keeps phytoplankton near the well-illuminated, warmer sea surface and is classically associated with high nutrient uptake and export[29]. The Eppley hypothesis remains controversial. Thermal Q_{10} effects on productivity, although perhaps real at high latitudes, are not supported at low latitudes[16], making it an unlikely mechanism to account for the inferred increase in deglacial productivity in lower latitude regions[7].

Subsurface warming would increase remineralization rates of organic matter sinking out of the near-surface ocean, and thus biological oxygen demand in the zone most sensitive to hypoxia. As with the first scenario, carbon export to the subsurface ocean, rather than primary productivity itself, would be the key variable, suggesting control by ecosystem effects that favour large diatoms (such as iron availability), or other effects on particle sinking rates. Thus both scenarios imply thermal triggers, but both require biogeochemical amplification to sustain subsurface hypoxia, plausibly through reductive iron remobilization on continental margins[19]. Such a feedback between ocean warming, OMZ expansion, and marine productivity may also provide a plausible mechanism to explain links between interstadial warm periods and abrupt transitions to hypoxia observed throughout the North Pacific[3,4,7,11], without the need to invoke changes in the Atlantic meridional overturning circulation and associated multi-century time lags of nutricline adjustment within the global ocean[8].

Projected future warming of the subpolar North Pacific will probably exceed the temperatures associated with past hypoxic events by the mid-twenty-first century[30], at sustained rates comparable to those preceding the deglacial hypoxic events. If enhanced biological productivity amplifies future deoxygenation as our evidence suggests it has in the past, substantial expansion of subsurface hypoxia beyond that predicted solely from thermal solubility effects may occur. While severe hypoxia would be catastrophic in the near-term for marine ecosystems and fisheries[18], the resulting reduction of carbon remineralization rates and enhanced burial of organic matter associated with hypoxia may also provide a long-term negative feedback on rising CO_2 and greenhouse-driven warming, as may have occurred during the deglacial hypoxic events[4] (Extended Data Fig. 9).

Online Content Methods, along with any additional Extended Data display items and Source Data, are available in the online version of the paper; references unique to these sections appear only in the online paper.

Received 9 February; accepted 17 September 2015.

1. Mix, A. C. *et al.* Rapid climate oscillations in the Northeast Pacific during the last deglaciation reflect Northern and Southern Hemisphere sources, in *Mechanisms of global climate change at millennial time scales, American Geophysical Union*, edited by P.U. Clark *et al.*, *Geophysical Monograph* **112,** 127–148 (1999).
2. Davies, M. H. *et al.* The deglacial transition on the southeastern Alaska Margin: Meltwater input, sea level rise, marine productivity, and sedimentary anoxia. *Paleoceanography* **26,** PA2223 (2011).
3. Behl, R. J. & Kennett, J. P. Brief interstadial events in the Santa Barbara basin, NE Pacific, during the past 60 kyr. *Nature* **379,** 243–246 (1996).
4. Jaccard, S. L. & Galbraith, E. D. Large climate-driven changes in oceanic oxygen concentrations during the last deglaciation. *Nature Geosci.* **5,** 151–156 (2012).

5. Okazaki, Y. *et al.* Deepwater formation in the North Pacific during the Last Glacial Termination. *Science* **329,** 200–204 (2010).
6. Crusius, J., Pedersen, T. F., Kienast, S., Keigwin, L. & Labeyrie, L. Influence of northwest Pacific productivity on North Pacific Intermediate Water oxygen concentrations during the Bølling-Allerød interval (14.7–12.9 ka). *Geology* **32,** 633–636 (2004).
7. Hendy, I. L., Pedersen, T. F., Kennett, J. P. & Tada, R. Intermittent existence of a southern Californian upwelling cell during submillennial climate change of the last 60 kyr. *Paleoceanography* **19,** PA3007 (2004).
8. Schmittner, A., Galbraith, E. D., Hostetler, S. W., Pedersen, T. F. & Zang, R. Large fluctuations of dissolved oxygen in the Indian and Pacific oceans during Dansgaard-Oeschger oscillations caused by variations of North Atlantic Deep Water subduction. *Paleoceanography* **22,** PA3207 (2007).
9. Kohfeld, K. E. & Chase, Z. Controls on deglacial changes in biogenic fluxes in the North Pacific ocean. *Quat. Sci. Rev.* **30,** 3350–3363 (2011).
10. Lam, P. J. *et al.* Transient stratification as the cause of the North Pacific productivity spike during deglaciation. *Nat. Geosci.* **6,** 622–626 (2013).
11. Kuehn, H. *et al.* Laminated sediments in the Bering Sea reveal atmospheric teleconnections to Greenland climate on millennial to decadal timescales during the last deglaciation. *Clim. Past* **10,** 2215–2236 (2014).
12. Barron, J. A., Bukry, D., Dean, W. E., Addison, J. A. & Finney, B. Paleoceanography of the Gulf of Alaska during the past 15,000 years: results from diatoms, silicoflagellates, and geochemistry. *Mar. Micropaleontol.* **72,** 176–195 (2009).
13. Addison, J. A. *et al.* Productivity and sedimentary $\delta^{15}N$ variability for the last 17,000 years along the northern Gulf of Alaska slope. *Paleoceanography* **27,** PA1206 (2012).
14. Keeling, R. F., Kortzinger, A. & Gruber, N. Ocean deoxygenation in a warming world. *Annu. Rev. Mar. Sci.* **2,** 199–229 (2010).
15. Schmittner, A., Oschlies, A., Matthews, H. D. & Galbraith, E. D. Future changes in climate, ocean circulation, ecosystems and biogeochemical cycling simulated for a business-as-usual CO_2 emission scenario until year 4000 AD. *Glob. Biogeochem. Cycles* **22,** GB1013 (2008).
16. Behrenfeld, M. J. *et al.* Climate-driven trends in contemporary ocean productivity. *Nature* **444,** 752–755 (2006).
17. Lopes, C., Kucera, M. & Mix, A. C. Climate change decouples oceanic primary and export productivity and organic carbon burial. *Proc. Natl Acad. Sci. USA* **112,** 332–335 (2014).
18. Diaz, R. J. & Rosenberg, R. Spreading dead zone and consequences for marine ecosystems. *Science* **321,** 926–929 (2008).
19. Scholz, F., McManus, J., Mix, A. C., Hensen, C. & Schneider, R. R. The impact of ocean deoxygenation on iron release from continental margin sediments. *Nat. Geosci.* **7,** 433–437 (2014).
20. Davies-Walczak, M. H. *et al.* Late glacial to Holocene radiocarbon constraints on North Pacific Intermediate Water ventilation and deglacial atmospheric CO_2 sources. *Earth Planet. Sci. Lett.* **397,** 57–66 (2014).
21. Takeda, S. Iron and phytoplankton growth in the subarctic North Pacific. *Aqua-BioScience Monographs* **4,** 41–93 (2011).
22. Benson, B. B. & Krause, D. J. The concentration and isotopic fractionation of oxygen dissolved in freshwater and seawater in equilibrium with the atmosphere. *Limnol. Oceanogr.* **29,** 620–632 (1984).
23. Hofmann, A. F. *et al.* Hypoxia by degrees: establishing definitions for a changing ocean. *Deep Sea Res. Part I Oceanogr. Res. Pap*. **58,** 1212–1226 (2011).
24. Ingall, E. & Jahnke, R. Evidence for enhanced phosphorus regeneration from marine sediments overlain by oxygen depleted waters. *Geochim. Cosmochim. Acta* **58,** 2571–2575 (1994).
25. Boyd, P. & Newton, P. Evidence of the potential influence of planktonic community structure on the interannual variability of particulate organic carbon flux. *Deep Sea Res. Part I Oceanogr. Res. Pap*. **42,** 619–639 (1995).
26. Hoffmann, L. J., Peeken, I., Lochte, K., Assmy, P. & Veldhuis, M. Different reaction of Southern Ocean phytoplankton size classes to iron fertilization. *Limnol. Oceanogr.* **51,** 1217–1229 (2006).
27. Kemp, A. E. S. & Villareal, T. A. High diatom production and export in stratified waters – A potential negative feedback to global warming. *Prog. Oceanogr.* **119,** 4–23 (2013).
28. Eppley, R. W. Temperature and phytoplankton growth in the sea. *Fish Bull.* **70,** 1063–1085 (1972).
29. Sverdrup, H. U. On conditions for the vernal blooming of phytoplankton. *ICES J. Mar. Sci.* **18,** 287–295 (1953).
30. Wang, M., Overland, J. E. & Bond, N. A. Climate projections for selected large marine ecosystems. *J. Mar. Syst.* **79,** 258–266 (2010).
31. Schlitzer, R. Electronic Atlas of WOCE Hydrographic and Tracer Data Now Available. *Eos Trans. AGU* **81,** 45 (2000).

Acknowledgements We thank J. Padman for assistance with faunal counts, K. Brewster for assistance with alkenone sample preparation and analysis, and A. Guiheneuf for preliminary alkenone measurements and faunal assemblage data. This work was supported by NSF grants AGS-0602395 (Project PALEOVAR, A.C.M.) and OCE-1204204 (A.C.M. and F.G.P.), and an NSF graduate research fellowship for S.K.P.; J.A.A. was supported by the USGS Climate and Land Use Change Research and Development Program and the Volcano Science Center.

Author Contributions S.K.P. and A.C.M. designed the study and wrote the paper. S.K.P., M.D.W., and F.G.P. contributed to alkenone palaeotemperature measurements and analysis. M.H.W. assisted with the chronology. J.A.A. provided insights on the trace metal and $\delta^{15}N$ records. All authors contributed to interpretation of the data and provided comments on the manuscript.

Author Information The data can be found in the supplementary online materials and at the National Oceanic and Atmospheric Administration Paleoclimate Database. Reprints and permissions information is available at www.nature.com/reprints. The authors declare no competing financial interests. Readers are welcome to comment on the online version of the paper. Correspondence and requests for materials should be addressed to S.K.P. (spraetorius@carnegiescience.edu).

METHODS

Sediment cores. Marine sediment core EW0408-85JC is located on the continental slope of the Gulf of Alaska (59° 33.32′ N, 144° 9.21′ W, 682 m). In the modern setting, this site lies near the upper margin of the OMZ, where oxygen concentrations are ~20 μmol kg^{-1} (Fig. 1). The Gulf of Alaska margin experiences high seasonal productivity during the spring and late summer months, with the highest chlorophyll levels observed along the northern margin[32], near the site of EW0408-85JC. The North Pacific drift feeds into the cyclonic Alaskan gyre and Alaskan Coastal Current (ACC), which drives downwelling along the margin[33]. Details and photographs of the sediment lithology for this core are previously published[2].

Several sediment cores from various depths from the Northeast Pacific were also employed for the compilation of an oxygen isotope depth transect. Site EW0408-26JC/TC lies along the continental slope off the southeast Alaska margin (56° 96′ N, 136° 43′ W, 1,623 m), near the lower boundary of the OMZ (Fig. 1). Site EW0408-87JC is located under the Gulf of Alaska subpolar gyre, at a depth that lies underneath the modern OMZ (58° 77′ N, 144° 50′ W, 3,680 m).

Age models. The age model for core EW0408-85JC is based on 36 radiocarbon dates of mixed planktonic foraminifera[20] calendar corrected using the Bayesian radiocarbon chronology program BChron[34] with the Marine13 database[35], assuming a marine reservoir correction of 880 ± 80 yr. The age models for cores EW0408-26JC/TC consist of 10 radiocarbon dates on mixed planktonic foraminifera, calibrated with Calib 7.0 using a marine reservoir correction of 735 ± 50 yr[36]. The age model for the trigger core of site EW0408-26 is poorly constrained due to low sedimentation rates, bioturbation, and carbonate dissolution in the upper sediments, therefore two tie points to the oxygen isotope stratigraphy of a nearby core with excellent age controls (EW0408-66JC) were used for the Holocene/YD boundary, and a modern age (0 yr BP) is assigned to the top of the core. The age model for core EW0408-87JC is based on 18 mixed planktonic radiocarbon dates calibrated with Calib 7.0 using a marine reservoir correction of 850 ± 100 yr (Extended Data Table 1). One sample was excluded from the age model due to a small reversal. The age model for ODP Site 1019[1] (Extended Data Fig. 1) is updated with the age model from Lopes *et al.*[17].

Ventilation estimates. Benthic radiocarbon ages were measured on mixed species of benthic foraminifera in the same samples as planktonic measurements to give an estimate of ventilation changes between the surface and deep waters at site EW0408-85JC[20]. Larger benthic-planktonic age differences reflect an increase in reservoir ages of subsurface waters, which may reflect either reduced ventilation rate, decreased preformed radiocarbon in the water mass, or mixing with an older water mass. Benthic ventilation ages were also evaluated using the projection age method[37], which accounts for changes in the atmospheric ^{14}C history based on the preformed radiocarbon content of surface waters before subduction, but does not account for subsurface mixing of multiple water masses.

Oxygen isotopes. Calculated $\delta^{18}O$ of seawater ($\delta^{18}O_{sw}$) combines planktonic $\delta^{18}O$ of Nps or Gb[2] with alkenone palaeotemperatures (this paper) using a Gb calibration equation[38], followed by correction for the global isotopic effect of changing ice volume[39].

The depth transect of $\delta^{18}O$ includes Nps $\delta^{18}O$ data from core EW0408-85JC[2] as representative of near-surface conditions. It includes benthic $\delta^{18}O$ representative of subsurface conditions in cores EW0408-85JC (682 m depth)[2] and EW0408-26JC/TC (1,623 m depth) from *Uvigerina peregrina* (Uvp), and in core EW0408-87JC (3,680 m depth) from *Cibicidoides wuellerstorfi* (+0.64 ‰). All were corrected for global ice volume[39], but not for temperature.

Alkenone palaeotemperature estimates. Total lipids were extracted from ~5 g of freeze-dried sediment as per Walinsky *et al.*[40]. Linear, alkenone-containing fractions were isolated via urea adduction[41] and analysed using capillary gas chromatography with flame ionization detection. Analytical uncertainties in the quantification of C_{37} ketone abundance (K37:2, K37:3 and K37:4) include both a mean potential 'baseline contaminant' component (positive) and an assumed 5% uncertainty in the integrated area (random). Minimum and maximum estimates of $U^{K'}_{37}$ {=(K37:2)/(K37:2 + K37:3)}[42] were determined from the uncertainty in K37:2 and K37:3 concentrations. The corresponding uncertainties in temperature estimates are large in samples in the deepest part of the core (corresponding in time to 17.5 – 17.0 ka) due to extremely low K37 concentrations, most likely related high sedimentation rates. Core-top alkenone palaeotemperatures are biased towards summer, and thus are representative of temperatures experienced by the photosynthetic source of these biomarkers[43].

Various studies have shown that different K37 compounds can be degraded selectively[44]. Consequently, the sea-surface water temperature proxy, $U^{K'}_{37}$, can be diagenetically biased to some extent. Most lines of evidence indicate preferential degradation of the more unsaturated K37:3. As a result, $U^{K'}_{37}$ values, if altered, typically are shifted positively, thereby depicting apparently warmer values. The magnitude of the documented diagenetic warming bias appeared to be ~1 °C or less under the extreme conditions of alkenone degradation experienced in the aerobic burn-down phenomena documented by turbidite records from the Madeira Abyssal Plain[45].

Bacteria capable of both selective and non-selective aerobic degradation of alkenones have been studied in the laboratory[46]. In cases where selective alkenone degradation led to a positive shift in $U^{K'}_{37}$ values, epoxide derivatives were measured as intermediate products of the process. An empirical calibration of the apparent diagenetic 'warming' effect on $U^{K'}_{37}$ values caused as a function of these epoxide intermediates has now been defined[45].

Alkenones and corresponding epoxide intermediates were measured in modern surface sediments collected by multi-core throughout our Southeast Alaska study area[43]. Interpretation of the results using the laboratory-defined empirical calibration suggested $U^{K'}_{37}$-based SST estimates were biased too warm by as much as 1–2.5 °C[43]. The perceived warming effect shows a weak correlation ($r = +0.26$) to the water depth at which each multi-core sample was collected, hinting that the magnitude of the warm bias is directly proportional to the availability of dissolved oxygen. Therefore, it is unlikely that estimated increases in SST during the hypoxic intervals in the Bølling–Allerød interstade (BA) and Holocene are related to changes in the sedimentary diagenetic environment. Observations of similar warming events during the BA and early Holocene from the California margin[47] (Extended Data Fig. 9) provide further support that these SST reconstructions reflect regional climate trends rather than local diagenetic imprints. Furthermore, the higher abundances of *Epistominella pacifica* relative to *Bolivina* and *Bulimina* species during cooling episodes in the SST reconstruction, such as the late glacial, Younger Dryas, and early to mid-Holocene (11–6 ka), suggest more oxygenated conditions during cool intervals. These trends are opposite of what would be expected if there was an influence of oxidation on the alkenone SST record, suggesting that a diagenetic warming effect, if present, would most likely act to dampen the observed magnitude of SST changes.

SST was also estimated via the U^{K}_{37} temperature index {=(K37:2 − K37:4)/(K37:2 + K37:3 + K37:4)} as calibrated by Prahl *et al.*[43] (Extended Data Fig. 2). The U^{K}_{37} index has been suggested to be a more reliable proxy for SST at temperatures below 8 °C[48,49]. The U^{K}_{37} index results in SST estimates that are ~4 °C colder during the late glacial period and ~1 °C warmer during the Holocene period relative to the $U^{K'}_{37}$ SST estimates, reflecting the influence of changes in the concentration of tetraunsaturated K37:4, which tends to have higher abundances during glacial times relative to interglacial times (Prahl *et al.*[50] and present study). However, the two SST estimates for the hypoxic intervals are virtually identical, providing further support that temperature estimates for these intervals are not influenced by preferential degradation of more unsaturated compounds. Additionally, the concentration of alkenones are highest during the hypoxic intervals (Extended Data Fig. 2), which not only increases the signal to noise ratio of our analyses (decreasing the associated SST errors), but is also consistent with excellent preservation of organic biomarkers during these events.

Average rates of SST change were calculated in a 400-yr window from the palaeotemperature record after interpolating on a 200-yr time step (Extended data Fig. 3)

Benthic faunal abundances. Benthic species abundances were counted from the >150 μm size fraction with sample splits that ranged from 25 – 400 benthic specimens (Extended data Fig. 4). Individual specimens were classified into 12 genera and species categories, and the percent abundance for each species was calculated relative to the total number of benthic species counted. *Bulimina* and *Bolivina* are both elongate infaunal benthic genera that are considered indicators of low-oxygen conditions, and sometimes associated with high export productivity[51–54]. *Bulimina exilis* is indicative of the most severe hypoxic/anoxic conditions[55]. *Epistominella pacifica* is an epifaunal species that can tolerate intermediate to strong hypoxia and are often found in the upper and lower boundary zones of OMZs[54]. *Uvigerina peregrina* can tolerate intermediate to weak hypoxia, but is typically absent from the core of the OMZ. Therefore the relative abundances of these species reflect changes in bottom water oxygen concentrations, with high abundances of *Uvigerina peregrina* reflecting relatively well-oxygenated conditions, *Epistominella pacifica* reflecting intermediate hypoxia, *Bolivina* genera reflecting strong hypoxia, and *Bulimina exilis* reflecting strongly hypoxic to anoxic conditions.

Trace metal data. Trace metal concentration data and methods are previously published[12,13]. Total metal concentration data (Me_T) of Mo and U was converted to excess (xs) values relative to lithogenic background, using Al concentration data in the core and the relationship: $Me_{xs} = Me_T - (Me/Al)_{lithogenic} \times Al_T$, using average continental crust values of $Mo/Al = 0.19 \times 10^{-4}$ and $U/Al = 0.35 \times 10^{-4}$ (ref. 19). Both raw concentration data and excess concentrations of Mo and U show similar trends, with the greatest enrichments of U and Mo during the hypoxic intervals.

Organic data. Biogenic silica and total organic carbon data and methods are previously published[2,13]. The $\delta^{15}N$ data and methods are previously published, along with a detailed discussion of various influences that may contribute to the bulk $\delta^{15}N$ signature[13]. A "corrected" marine $\delta^{15}N$ record was also calculated by

correcting for the $\delta^{15}N$ component imparted from terrestrial organic matter[13] (Extended Data Fig. 5). This record shows similar overall trends to the raw $\delta^{15}N$ record, with enriched $\delta^{15}N$ during the BA and early Holocene hypoxic events. Elevated $\delta^{15}N$ during the hypoxic intervals is consistent with an increase in nutrient utilization rate, which in this iron-limited setting would likely require an elevated iron source.

The $\delta^{15}N$ data alone do not prove nutrient utilization; an alternate interpretation is that the high $\delta^{15}N$ events during the deglacial transition are an advected signal from low latitudes, where a stronger oxygen minimum zone resulted in water column denitrification[56]. The viability of the undercurrent transport hypothesis is supported by modern tracer distributions that show California Undercurrent water detectable as far north as Alaska[57]. Addison *et al.*[13] discounted the undercurrent transport hypothesis as an explanation for deglacial increases in $\delta^{15}N$, simply because the fraction of undercurrent water reaching Alaska today is small (<15% of the subsurface water mass). Implausibly high variations in the tropical source waters (>12 ‰) would be required to explain the ~2‰ $\delta^{15}N$ changes in the Gulf of Alaska; such large changes have not been observed in the eastern tropical Pacific[58]. There is no dynamical mechanism to explain large increases in net pole-ward transport relative to mixing with ambient waters along the flow path that could yield such high-amplitude $\delta^{15}N$ changes in the Gulf of Alaska.

Additional data argues in favour of a nutrient utilization mechanism to explain the high $\delta^{15}N$ events in the Gulf of Alaska. Planktonic foraminiferal $\delta^{13}C$ rises during the Bølling–Allerød and early Holocene warming events, sympathetic with high $\delta^{15}N$ events (Extended Data Figs 5 and 6). If the $\delta^{15}N$ were explained entirely by increased northward advection of high-nutrient, low-oxygen undercurrent waters from the tropics, the warm events should be accompanied by anomalously low $\delta^{13}C$ of dissolved inorganic carbon. The same conflict appears for explanations of high productivity by upwelling of deep nutrient rich waters at these times[9]; upwelling of nutrient-rich waters without an increase in fractional nutrient utilization would yield low $\delta^{13}C$ (Extended Data Fig. 6).

A regime change occurs in the early Holocene, from a deglacial interval in which $\delta^{15}N$ is positively correlated with $\delta^{13}C$ (17–9 ka, $r^2 = 0.51$) to a Holocene system in which $\delta^{15}N$ and $\delta^{13}C$ are weakly negatively correlated (Extended Data Fig. 6). Consideration of changes in atmospheric $\delta^{13}C$ (ref. 59) and air-sea equilibrium of the $\delta^{13}C$ of carbonate ion as a function of temperature[60] strengthens this relationship (Extended Data Fig. 6). The co-occurrence of high $\delta^{13}C$ with high $\delta^{15}N$ during the deglacial interval points to nutrient utilization rate and carbon export as a key driver of the hypoxic events.

This view of nutrient utilization, likely related to removal of iron limitation during the deglacial interval is not inconsistent with the general view of advection of low-oxygen waters northward in the California Undercurrent. Indeed, northward advection of such low oxygen waters near the shelf-slope break would provide a potential reductive source of iron and phosphate[24] from sediments, and would be part of a self-sustaining feedback in the northeast Pacific in which initial hypoxia would be sustained and strengthened by iron-fuelled export productivity. Iron can be transported relatively long distances in the subsurface ocean in the colloidal (essentially non-sinking) fraction[61]. Such a mechanism is consistent with sea-level rise onto the continental shelves as a possible iron source[1], and addresses concerns that isostatic rebound puts the local sea-level record in the northern Gulf of Alaska out of synch with the hypoxic events[9].

Leads/lags in proxy data. The collection of multiple proxies within the same core allows for a precise examination of the timing of redox changes relative to changes in oceanographic conditions and export productivity (Extended Data Fig. 7). The transition to laminated sediments during the BA occurs with a sharp sedimentological boundary at 681 cm core depth[2]. The laminations are closely associated with high weight percentages of biogenic opal, consistent with high export of diatoms. The laminated intervals are also clearly defined in the X-ray computed tomography (CT) grey scan data, which largely tracks sediment density as a function of the biogenic to lithogenic fraction, with low values indicating times of high biogenic input[2]. The initial increase in SST precedes the increase in opal and the onset of laminations during the BA hypoxic event; temperatures >10 °C are associated with the interval of high diatom abundances. The increase in U and Mo occurs slightly before (2 – 5 cm) the increases in biogenic opal, TOC, and the decrease in CT grey scale. This may reflect a progression towards low oxygen conditions before the increase in export productivity. It is possible that such small depth offsets between the increase in trace metals and organic matter concentration may reflect preserved redox gradients in the sediment column, and thus not truly represent offsets in the time domain. However, all these proxies are emplaced within the bioturbed mixed layer and within a few cm of the seafloor during laminated intervals[62], so depth offsets between proxies should be minor.

There are no discernible leads or lags between the increase in SST and export productivity for the Holocene hypoxic event. However, in this interval, the increase in U and Mo appear to slightly lag the increase in biogenic silica and the transition to low-oxygen benthic fauna. The Holocene laminated interval is not as precisely defined as the onset of the BA laminations, partly due to weaker (slightly mottled) laminations, making the evaluation of depth offsets in the proxy data less reliable than for the BA sequence.

The switch from oxic to hypoxic/anoxic-tolerant benthic fauna occurs abruptly near the onset of laminations for both the BA and Holocene events. However, low-oxygen benthic species dominate the faunal assemblages well after the termination of laminations and the decrease in biogenic silica. Similar trends can be seen in the trace metal data. This concordance may indicate that low-oxygen conditions persisted even after the decline in export productivity and the cessation of laminations. This is consistent with a hysteresis-like response in the benthos, with an abrupt threshold transition to a hypoxic regime, followed by a more gradual return to an oxic regime with a diversity of benthic fauna[63]. Some upward mixing of older hypoxic fauna by bioturbation could have occurred when oxic conditions returned, however, this is unlikely to account for the high abundances (60 – 80%) of low-oxygen fauna that persisted in these intervals.

Based on this sequence of events, it appears most probable that sea surface warming lead to a reduction of dissolved oxygen in the subsurface through the combined effects of reduced oxygen solubility and enhanced thermal stratification. Benthic fauna assemblages from a deeper site in the Gulf of Alaska (near the lower boundary of the OMZ) suggest a gradual progression towards hypoxia starting at 16 ka, followed by an abrupt onset of laminations at the transition into the BA (Extended Data Fig. 8). The initial reduction of dissolved oxygen in the subsurface would have intensified the OMZ, leading to an expanded area of hypoxic shelf sediments (Fig. 3). A shoaling of the upper boundary of the OMZ to ~300 m during the BA hypoxic event has been documented in benthic faunal assemblages from the California Borderland basins[64].

The supply of sedimentary iron is thought to be most efficient in a redox window where neither oxygen nor sulfide is present[19], making such "new hypoxic zones" prime candidates for the release of bioavailable iron, especially in the shallower depths where iron can be more easily upwelled to the surface, as occurs in offshore regions of the Gulf of Alaska. Additional sources of iron include freshwater runoff charged with glacial rock flour. Such supplies of iron could have helped to fuel primary productivity, enhanced export productivity, and further depleted subsurface ocean concentrations, leading to a threshold-like feedback effect to amplify ocean deoxygenation.

Feedbacks on the carbon cycle. The timing of the North Pacific hypoxic events approximately coincided with two intervals of abrupt increase in atmospheric N_2O (ref. 65) and a cessation in the rise of atmospheric CO_2 (refs 66, 67) (Extended Data Fig. 9). The widespread expansion of hypoxic zones in the North Pacific could have led to denitrification, contributing to the two abrupt increases in atmospheric N_2O, while the enhanced export flux and burial of organic carbon may have helped to stabilize the rise in atmospheric CO_2 (ref. 4). Thus, the temperature evolution of the North Pacific could play a prominent role in the regulation of multiple greenhouse gases.

Initial deglacial warming could promote out-gassing of deep-ocean respired carbon. Continuous and/or abrupt warming could have pushed large areas of the North Pacific across thresholds of hypoxia, in which the cycling of nutrients and carbon was fundamentally altered, contributing to expansive denitrification and the release of N_2O gases. However, the development of widespread hypoxia may ultimately act as a negative feedback on rising CO_2 and global warming, with the release of nutrients from hypoxic sediments acting to stimulate surface productivity (in particular, diatoms with high efficiency for carbon export[27]) and the decrease in water column oxygen concentration helping to promote carbon burial (Fig. 3). Thus, thresholds of hypoxia in the North Pacific linked to ocean warming have the potential to switch this region from a source to sink of carbon.

32. Brickley, P. J. & Thomas, A. C. Satellite-measured seasonal and inter-annual chlorophyll variability in the Northeast Pacific and Coastal Gulf of Alaska. *Deep Sea Res. Part II Top. Stud. Oceanogr.* **51,** 229–245 (2004).
33. Stabeno, P. J. *et al.* Meteorology and oceanography of the Northern Gulf of Alaska. *Cont. Shelf Res.* **24,** 859–897 (2004).
34. Parnell, A. C. *et al.* A flexible approach to assessing synchroneity of past events using Bayesian reconstructions of sedimentation history. *Quat. Sci. Rev.* **27,** 1872–1885 (2008).
35. Reimer, P. J. *et al.* INTCAL13 and MARINE13 radiocarbon age calibration curves, 0–50,000 years cal BP. *Radiocarbon* **55,** 1869–1887 (2013).
36. Praetorius, S. K. & Mix, A. C. Synchronization of North Pacific and Greenland climates preceded abrupt deglacial warming. *Science* **345,** 444–448 (2014).
37. Adkins, J. F. & Boyle, E. A. Changing atmospheric $\Delta^{14}C$ and the record of deep water paleoventilation ages. *Paleoceanography* **12,** 337–344 (1997).
38. Bemis, B. E., Spero, H. J., Bijima, J. & Lea, D. W. Reevaluation of the oxygen isotopic composition of planktonic foraminifera: Experimental results and revised paleotemperature equations. *Paleoceanography* **13,** 150–160 (1988).

39. Waelbroeck, C. L. *et al.* Sea-level and deep water temperature changes derived from benthic foraminifera isotopic records. *Quat. Sci. Rev.* **21,** 295–305 (2002).
40. Walinsky, S. E. *et al.* Distribution and composition of organic matter in surface sediments of coastal Southeast Alaska. *Cont. Shelf Res.* **29,** 1565–1579 (2009).
41. Christie, W. W. & Han, X. *Lipid Analysis: Isolation, Separation, Identification and Structural Analysis of Lipids* 4th edn (Oily Press, 2003)
42. Prahl, F. G., Muehlhausen, L. A. & Zahnle, D. L. Further evaluation of long-chain alkenones as indicators of paleoceanographic conditions. *Geochim. Cosmochim. Acta* **52,** 2303–2310 (1988).
43. Prahl, F. G. *et al.* Systematic pattern in $U^{K'}_{37}$ – Temperature residuals for surface sediments from high latitude and other oceanographic settings. *Geochim. Cosmochim. Acta* **74,** 131–143 (2010).
44. Rontani, J. F., Volkman, J. K., Prahl, F. G. & Wakeham, S. G. Biotic and abiotic degradation of alkenones and implications on $U^{K'}_{37}$ paleoproxy application. *A review. Org. Geochem*. **59,** 95–113 (2013).
45. Prahl, F. G., Cowie, G. L., De Lange, G. J. & Sparrow, M. G. Selective organic matter preservation in "burn-down" turbidites on the Madeira Abyssal Pla in. *Paleoceanography* **18,** 1052 (2003)
46. Rontani, J. F. *et al.* Degradation of alkenones by aerobic heterotrophic bacteria: selective or not? *Org. Geochem.* **39,** 34–51 (2008).
47. Barron, J. A., Heusser, L., Herbert, T. & Lyle, M. High-resolution climatic evolution of coastal northern California during the past 16,000 years. *Paleoceanography* **18,** 1020 (2003).
48. Roselle-Melé, A. & Comes, P. Evidence for a warm Last Glacial Maximum in the Nordic seas or an example of shortcomings in $U^{K}_{37'}$ and U^{K}_{37} to estimate low seas surface temperature? *Paleoceanography* **14,** 770–776 (1999).
49. Bendle, J. & Roselle-Mele, A. Distributions of U^{K}_{37} and $U^{K}_{37'}$ in the surface waters and sediments of the Nordic Seas: Implications for paleoceanography. *Geochem. Geophys. Geosyst.* **5,** Q11013 (2004).
50. Prahl, F. G. *et al.* Assessment of sea-surface temperature at 42°N in the California Current over the last 30,000 years. *Paleoceanography* **10,** 763–773 (1995).
51. Bernhard, J. M. Characteristic assemblages and morphologies of benthic foraminifera from anoxia, organic-rich deposits: Jurassic through Holocene. *J. Foraminiferal Res.* **16,** 207–215 (1986).
52. Bernhard, J. & Reimers, C. Benthic foraminiferal population fluctuation related to anoxia: Santa Barbara Basin. *Biochemistry* **15,** 127–149 (1991).
53. Kaiho, K. Benthic foraminiferal dissolved-oxygen index and dissolved-oxygen levels in the modern ocean. *Geology* **22,** 719–722 (1994).
54. Jorissen, F. J., Fontanier, C. & Thomas, E. Paleoceanographical proxies based on deep-sea benthic foraminiferal assemblage characteristics. Proxies in Late Cenozoic Paleoceanography: Pt. 2: Biological tracers and biomarkers (eds Hillaire-Marcel C. & de Vernal, A.) 263–326 (Elsevier, 2007)
55. Hermelin, J. O. R. & Shimmield, G. B. The importance of the oxygen minimum zone and sediment geochemistry on the distribution of recent benthic foraminifera from the NW Indian ocean. *Mar. Geol.* **91,** 1–29 (1990).
56. Kienast, S. S., Calvert, S. E. & Pedersen, T. F. Nitrogen isotope and productivity variations along the northeast Pacific margin over the last 120 kyr: surface and subsurface paleoceanography. *Paleoceanography* **17,** 7-1–7-17 (2002).
57. Thomson, R. E. & Krassovski, M. V. Poleward reach of the California Undercurrent extension. *J. Geophys. Res.* **115,** C09027 (2010).
58. Robinson, R. S., Martinez, P., Pena, L. D. & Cacho, I. Nitrogen isotopic evidence for deglacial changes in nutrient supply in the eastern equatorial Pacific. *Paleoceanography* **24,** PA4213 (2009).
59. Schmitt, J. *et al.* Carbon isotope constraints on the deglacial CO_2 rise from ice cores. *Science* **336,** 711–714 (2012).
60. Zhang, J., Quay, P. D. & Wilbur, D. O. Carbon isotope fractionation during gas water exchange and dissolution of CO_2. *Geochim. Cosmochim. Acta* **59,** 107–114 (1995).
61. Fitzsimmons, J. N., Boyle, E. A. & Jenkins, W. J. Distal transport of dissolved hydrothermal iron in the deep South Pacific Ocean. *Proc. Natl Acad. Sci. USA* **111,** 16654–16661 (2014).
62. Chang, A. S., Pichevin, L., Pedersen, T. F., Gray, V. & Ganeshram, R. New insights into productivity and redox-controlled trace element (Ag, Cd, Re, and Mo) accumulation in a 55 kyr long sediment record from Guaymas Basin, Gulf of California. *Paleoceanography* **30,** 77–94 (2015).
63. Conley, D. J., Carstensen, J., Vaquer-Sunyer, R. & Duarte, C. M. Ecosystem thresholds with hypoxia. *Hydrobiologia* **629,** 21–29 (2009).
64. Moffitt, S. E., Hill, T. M., Ohkushi, K., Kennett, J. P. & Behl, R. Vertical oxygen minimum zone oscillations since 20 ka in Santa Barbara Basin: A benthic foraminiferal community perspective. *Paleoceanography* **29,** 44–57 (2014).
65. Schilt, A. *et al.* Atmospheric nitrous oxide during the last 140,000 years. *Earth Planet. Sci. Lett.* **300,** 33–43 (2010).
66. Monnin, E. *et al.* Atmospheric CO_2 concentrations over the last glacial termination. *Science* **291,** 112–114 (2001).
67. Marcott, S. A. *et al.* Centennial-scale changes in the global carbon cycle during the last deglaciation. *Nature* **514,** 616–619 (2014).
68. Hill, T. M. *et al.* Pre-Bølling warming in Santa Barbara Basin, California: surface and intermediate water records of early deglacial warmth. *Quat. Sci. Rev.* **25,** 2835–2845 (2006).

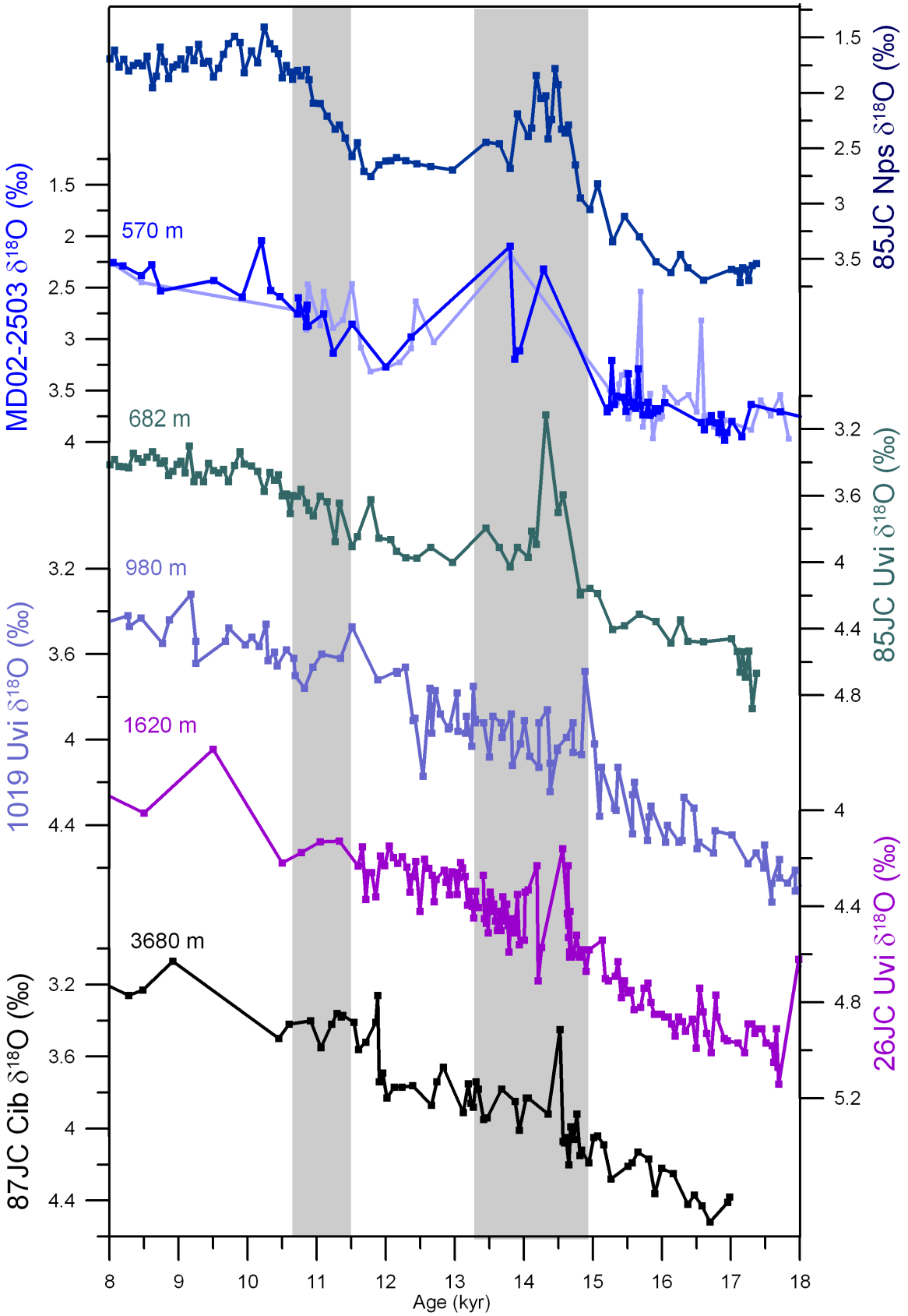

Extended Data Figure 1 | Depth transect of oxygen isotopes from the Northeast Pacific. Planktonic oxygen isotopes (Nps) from core EW0408-85JC (dark blue)[2], benthic oxygen isotopes from core MD02-2503 in the Santa Barbara basin (*Uvigerina peregrina*; light blue, *Bolivina argentea*; bright blue)[68], benthic *Uvigerina peregrina* oxygen isotopes from core EW0408-85JC (green)[2], ODP Site 1019 ((41° 68′ N, 124° 93′ W, 978 m; light blue)[1], cores EW0408-26JC/TC, and core EW0408-87JC (*Cibicidoides*). Data from the Gulf of Alaska cores (EW0408) are used to make the depth-time map shown in Fig. 4.

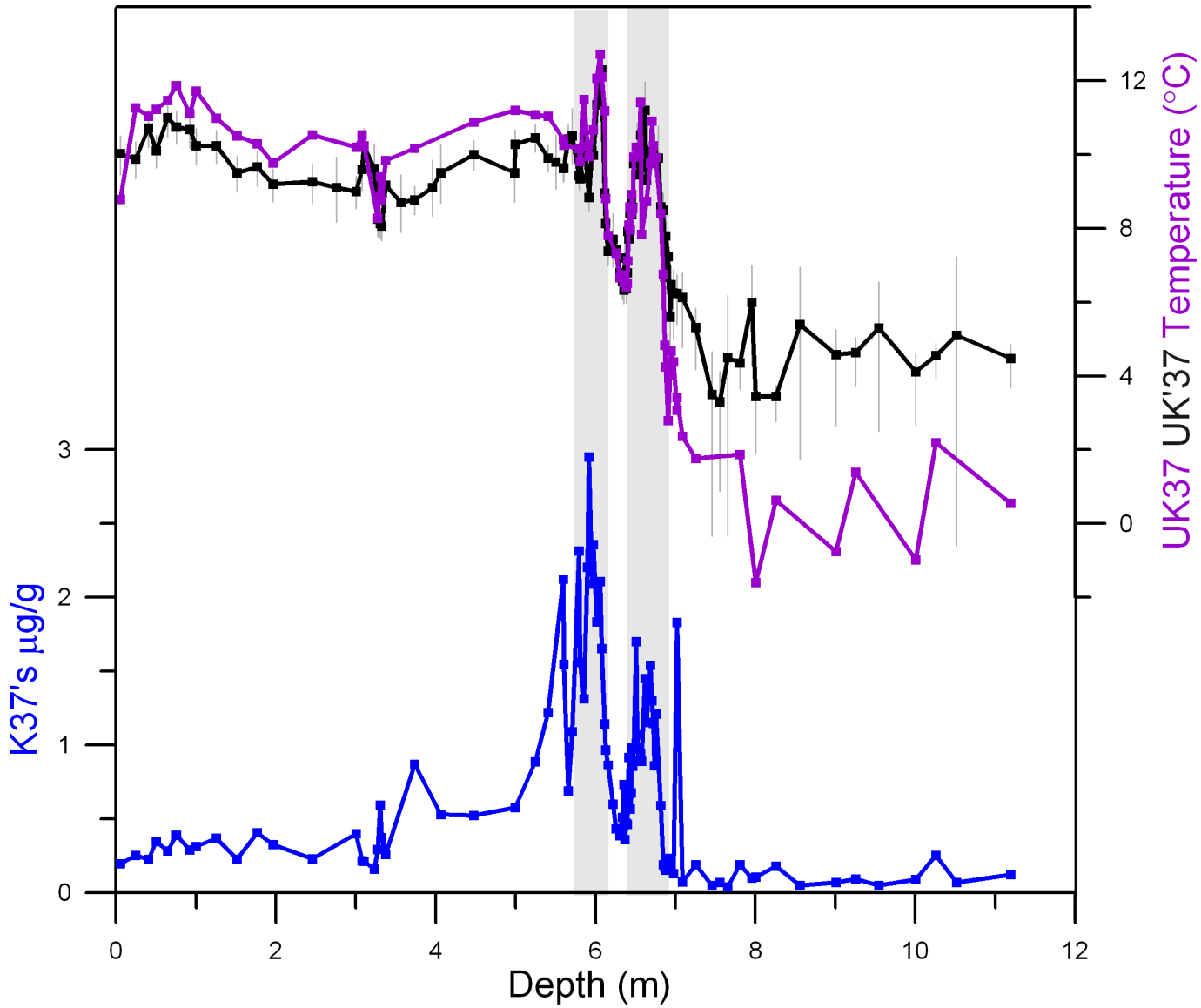

Extended Data Figure 2 | Comparison of SST estimates based on the U_{37}^{K} (purple) and $U_{37}^{K'}$ (black) indices. Temperatures based on the U_{37}^{K} index show a larger glacial-interglacial change, with colder SSTs during the late glacial period and warmer SST for the Holocene. Temperature estimates for the deglacial period, including the two hypoxic intervals and the Younger Dryas, are virtually identical between methods, giving confidence that diagenetic effects are not influencing the alkenone ratios during the hypoxic warm events. Alkenone concentrations are high during the two hypoxic events (blue), consistent with other proxy evidence for high productivity and/or excellent preservation of organic matter during these events.

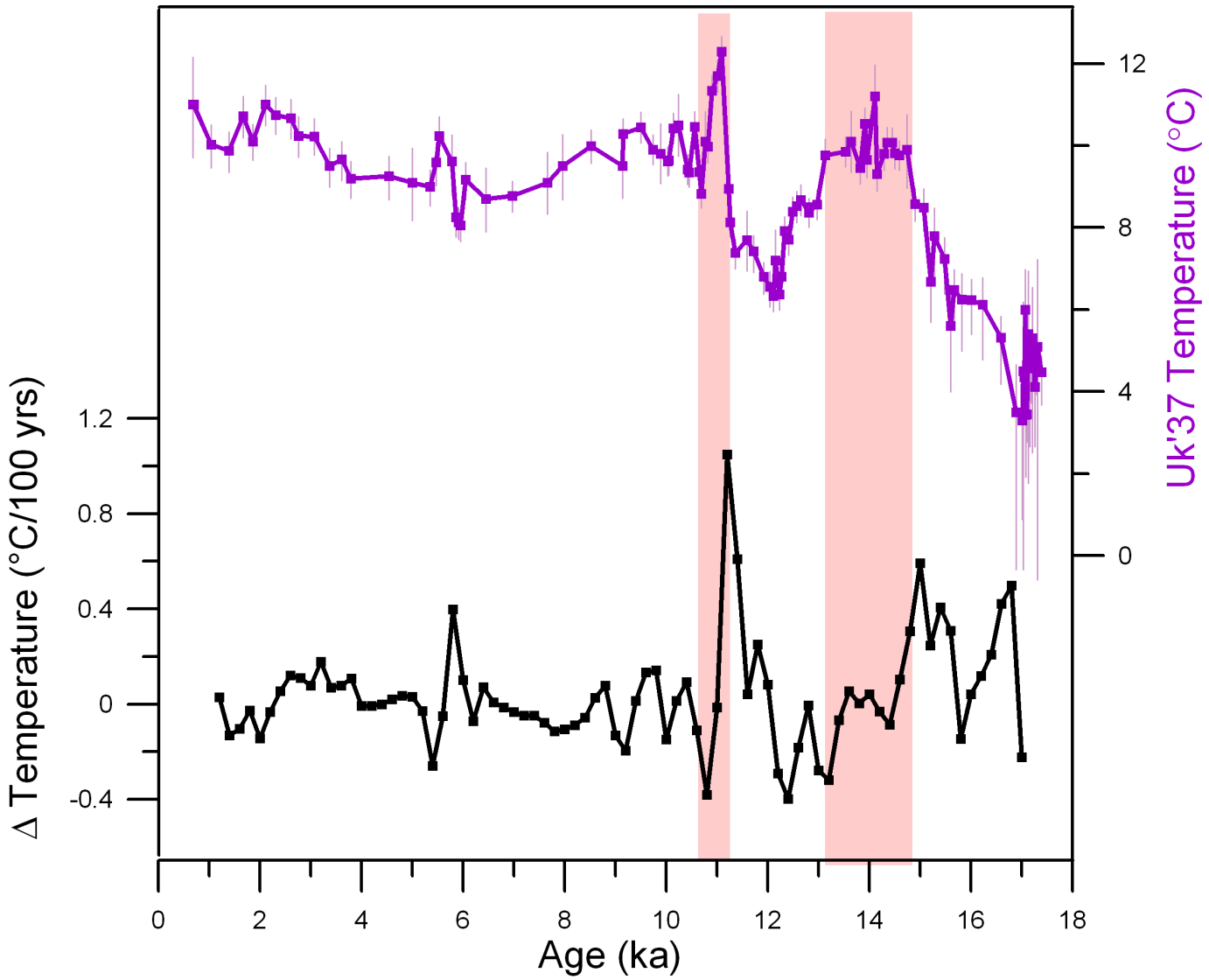

Extended Data Figure 3 | Rate of SST change in the Gulf of Alaska. The alkenone palaeotemperature record (purple) was interpolated on a 200-yr time step and the average rate of temperature change (°C per century) was calculated over a 400-yr window (black).

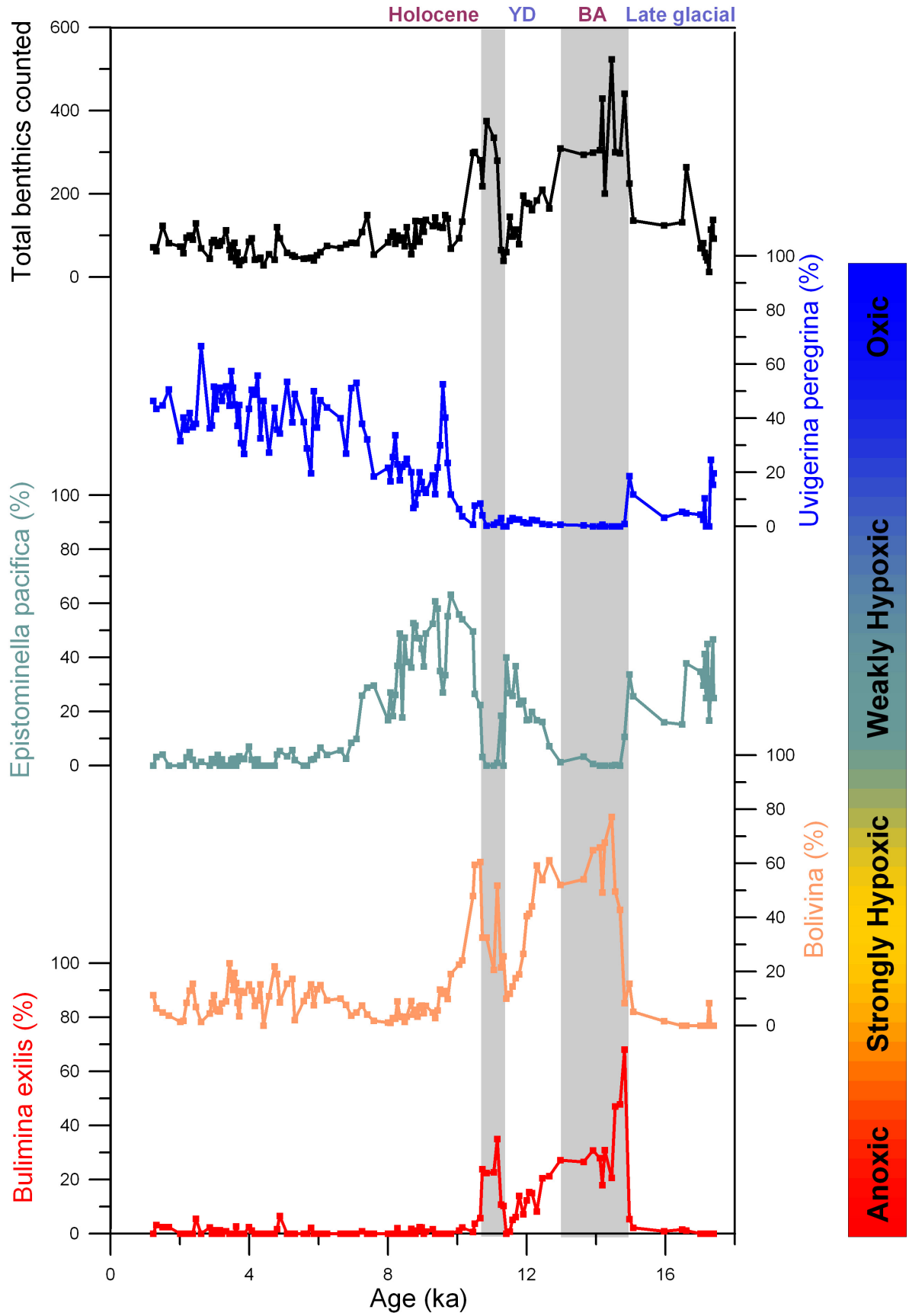

Extended Data Figure 4 | Relative abundances of benthic species and genera in core EW0408-85JC. *Bulimina exilis* is the most tolerant of low-oxygen conditions, and is often associated with near-anoxic bottom waters. *Bulimina* and *Bolivina* genera are typically found in strongly hypoxic waters, whereas *Epistominella pacifica* is associated with intermediate hypoxia, and *Uvigerina peregrina* is associated with more well-oxygenated conditions. Grey shaded bars represent the two laminated intervals, which are almost exclusively comprised of *Bolivina* and *Bulimina* genera.

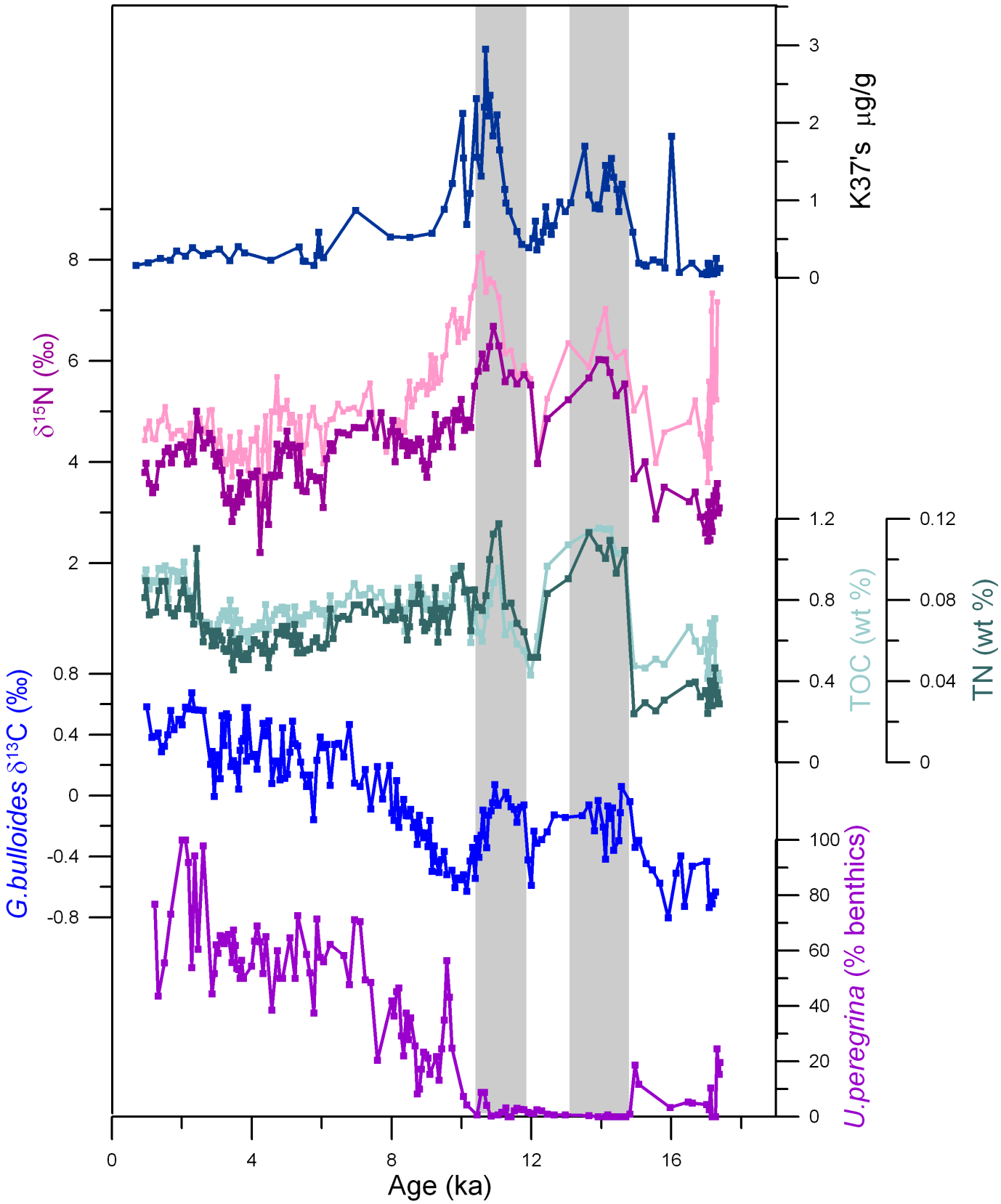

Extended Data Figure 5 | Records of surface and export productivity from EW0408-85JC. The sedimentary $\delta^{15}N$ record (violet) and $\delta^{15}N$ corrected for terrestrial organic matter (light violet)[13] show elevated values during the two hypoxic intervals (grey bars), which also coincide with enhanced organic matter deposition, including total organic carbon (light green)[13] and an increase in the alkenone K37 abundance (dark blue). High planktonic $\delta^{13}C$ values are observed during these intervals (bright blue)[2], consistent with an increase in surface productivity rather than upwelling of deep waters exported from low-latitudes. The progressive increase in planktonic $\delta^{13}C$ through the Holocene is accompanied by an increase in the relative abundance of *U. peregrina* (purple), likely indicating a better ventilated water column in the Holocene.

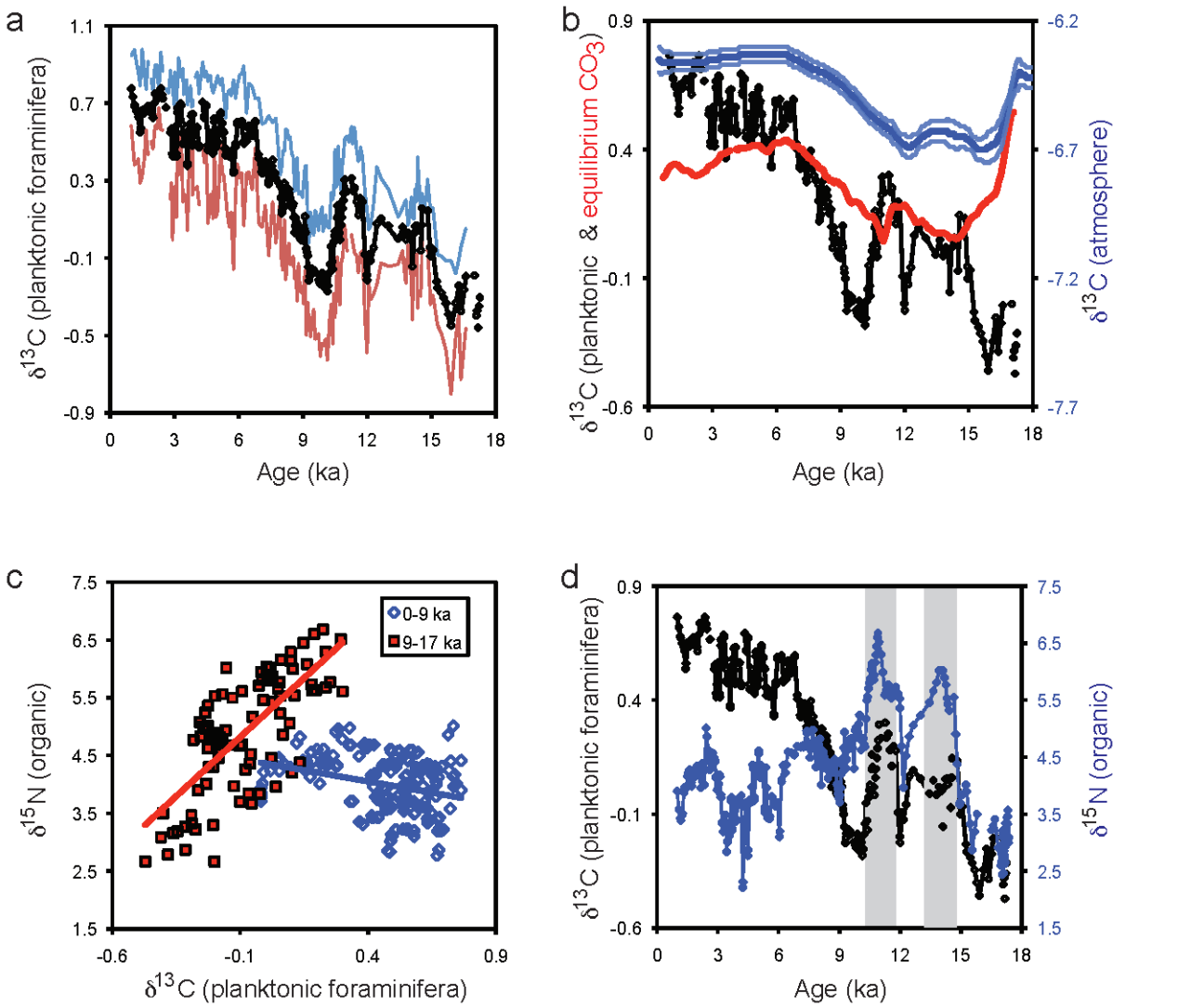

Extended Data Figure 6 | Comparison of planktonic $\delta^{13}C$ with sedimentary $\delta^{15}N$ in core EW0408-85JC. a, $\delta^{13}C$ of planktonic foraminifera, Nps (blue), Gb (red), average of the two species (black). **b**, Comparison of the average planktonic foraminiferal $\delta^{13}C$ (black) with changes in $\delta^{13}C$ of atmospheric CO_2 (blue)[57] and estimated surface ocean $\delta^{13}C$ of $CO_3^=$. (red, calculated from the smooth atmospheric values using the temperature relationship of Zhang *et al.*[60] **c**, Relationship between $\delta^{15}N$ in organic matter and $\delta^{13}C$ in planktonic foraminifera (average of Gb and Nps). The $\delta^{15}N$ and $\delta^{13}C$ measurements were in most cases made in adjacent samples, typically separated by 1 cm. To prevent directional bias in the scatter plot, the two variables were first interpolated linearly onto the depth of the other variable. In no cases were interpolations allowed over an interval >5 cm or 200 years. The positive correlation between organic $\delta^{15}N$ and planktonic foraminiferal $\delta^{13}C$ during the deglacial interval (17–9 ka, red points, $r^2 = 0.51$) supports an interpretation of increased nutrient utilization and carbon export from near-surface waters associated with the high $\delta^{15}N$ events. In contrast, within Holocene time (9–0 ka) the relationship between $\delta^{15}N$ and $\delta^{13}C$ reverses, suggesting no systematic variations in nutrient utilization. **d**, Time series of organic $\delta^{15}N$ (organic) and $\delta^{13}C$ (average of the planktonic foraminifera Gb and Nps) as a time series; these data form the comparison in **c**.

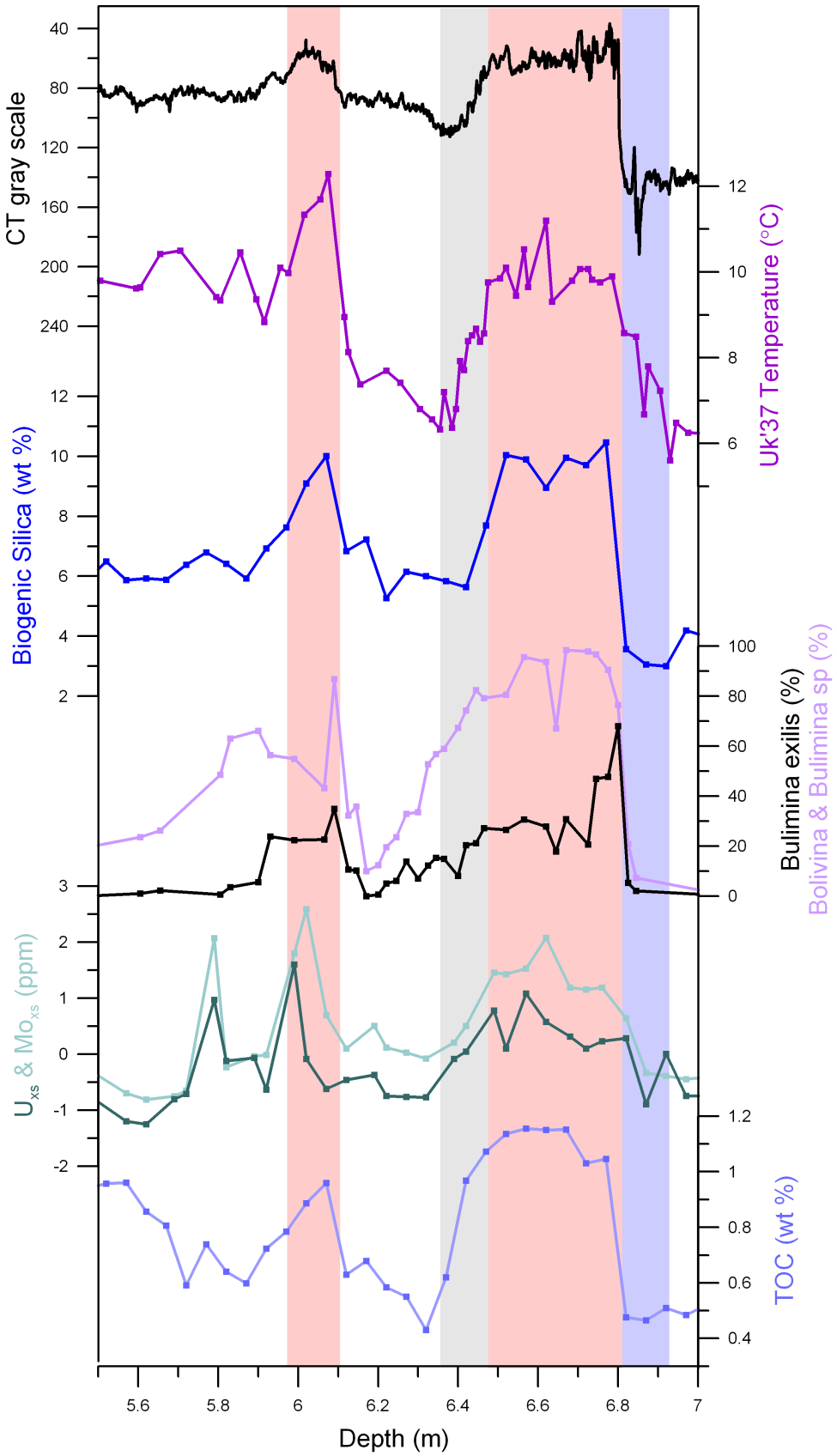

Extended Data Figure 7 | Expanded view of proxy data (plotted as depth in core) for EW0408-85JC during the two hypoxic intervals. CT grey scale (black) reflects changes in the biogenic:lithogenic fraction of sediment, with low values indicating times of high biogenic input (primarily diatoms)[2]. The laminated intervals (pink shading) coincide with high diatom abundance and SSTs near or exceeding 10 °C, whereas evidence for low-oxygen conditions appears to extend both before (blue shading) and after (grey shading) the BA laminated zone based on trace metal concentrations[12,13], benthic faunal assemblages, and preservation of TOC[13], coinciding with the initial increase in SST and decrease in benthic $\delta^{18}O$ (dark blue)[2].

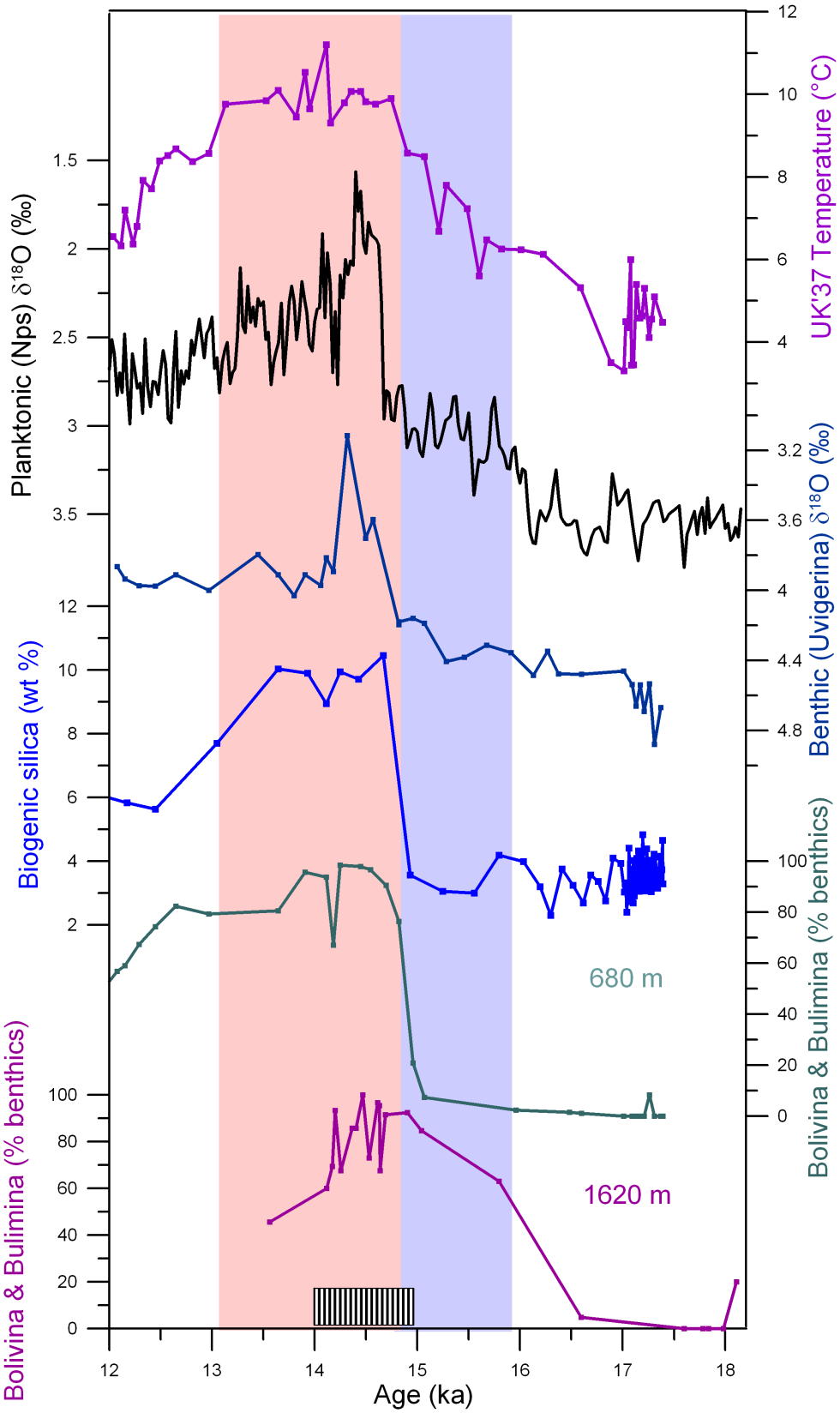

Extended Data Figure 8 | Surface climate proxies compared with changes in benthic $\delta^{18}O$ and fauna from different depth sites in the Gulf of Alaska. The alkenone palaeotemperature record from core EW0408-85JC (purple), a composite record of planktonic $\delta^{18}O$ from cores EW0408-26JC and EW0408-66JC (black)[36], benthic $\delta^{18}O$ (dark blue) and biogenic silica (bright blue) from core EW0408-85JC[2], the combined abundance of low-oxygen tolerant *Bolivina* and *Bulimina* species from cores EW0408-85JC (682 m; green) and EW0408-26JC (1,620 m; violet). An increase in low-oxygen benthic fauna is apparent in the deeper site (EW0408-26JC) commencing at 16 ka, which coincides with the pre-Bølling warming in the SST record and an increase in the planktonic and benthic $\delta^{18}O$ records. This initial decrease (blue shading) in sedimentary oxygen content at the base of the OMZ clearly precedes the large increase in biogenic silica and the shift to hypoxic conditions in core EW0408-85JC near the onset of sedimentary laminations (pink shading). Sediment laminations in core EW0408-26JC occur from 15–14 ka (shaded bar on *x*-axis).

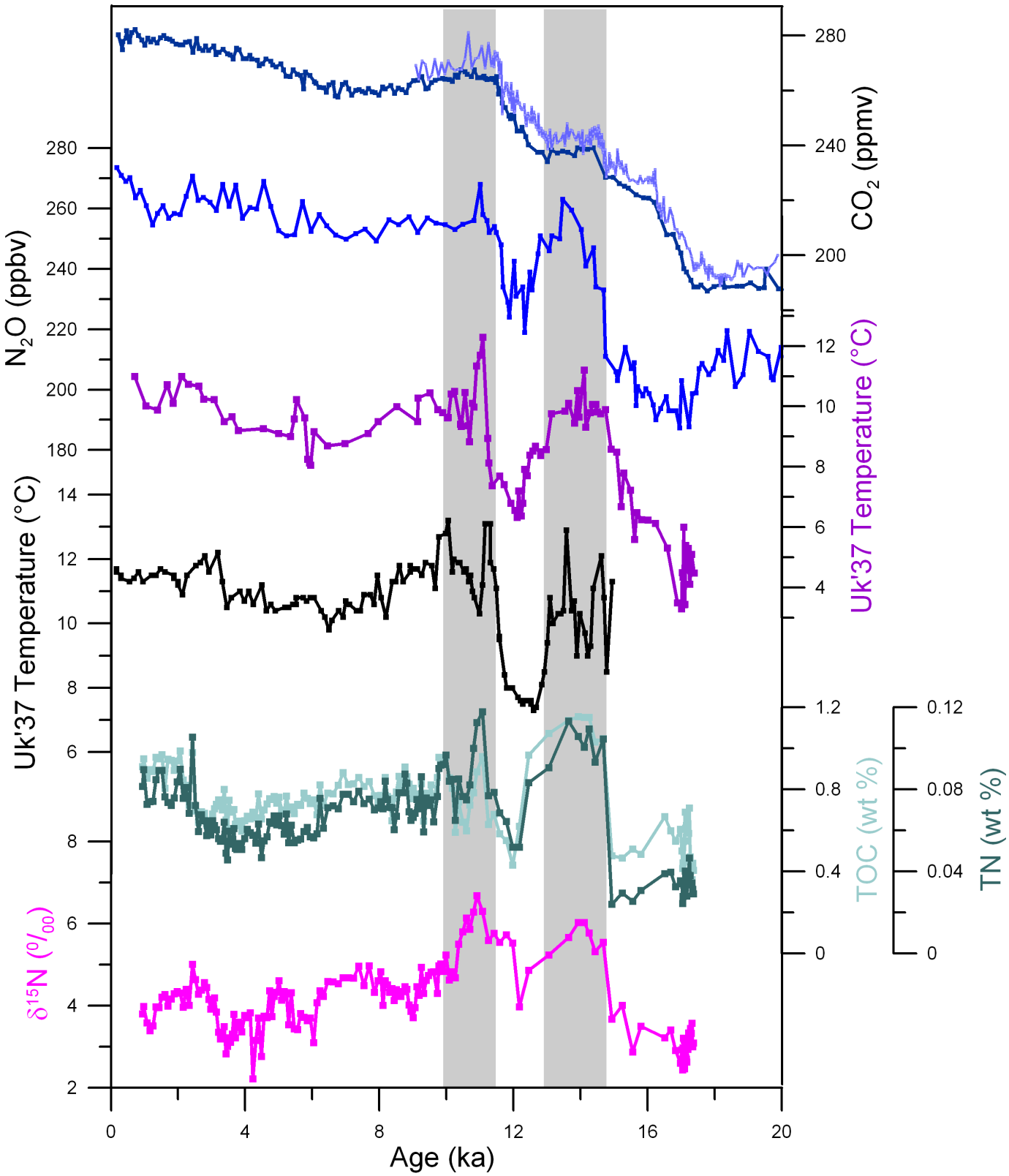

Extended Data Figure 9 | Northeast Pacific SSTs, productivity indices, and atmospheric greenhouse gases. Data from top: CO_2 record from EDC (dark blue)[66] and WAIS (light blue)[67], a record of N_2O from TALOS Dome (bright blue)[65], the Gulf of Alaska $U^{K'}_{37}$ SST record (purple), a $U^{K'}_{37}$ SST record from the California margin (black)[47], records of total organic carbon (TOC: light green), total nitrogen (TN: dark green), and $\delta^{15}N$ records on bulk organic matter from core EW0408-85JC[13]. Grey shaded bars indicate the two intervals in which the deglacial rise in CO_2 plateaus/reverses, which generally correspond to the episodes of widespread North Pacific hypoxia, high SSTs, enhanced nitrate utilization, and increased export productivity.

Extended Data Table 1 | Radiocarbon age controls for core EW0408-87JC

Depth midpoint (cm)	Planktonic ^{14}C age (yr)	^{14}C +/- (yr)	Marine13 age (yr)	2 sigma error (yr)
39.0	1640	15	760	110
208.5	8520	20	8530	140
245.0	10715	20	11330	160
250.0	10740	40	11380	240
255.0	10975	30	11700	300
267.0	11090	25	11990	280
281.0	11695	30	12740	130
301.0	12460	40	13470	160
329.0	13170	40	14370	320
341.0	13330	45	14650	400
381.0	13830	30	15510	230
420.5	14290	40	16160	230
460.0	14560	70	16570	310
492.0	14840	70	16950	330
540.0	14930	60	17120	300
920.0	15060	45	17300	220
1002.0	15020	50	17250*	240
1449.0	15445	40	17770	190

Radiocarbon measurements were made on mixed planktonic foraminifera, sinistral *Neogloboquadrina pachyderma* (Nps) and *Globigerina bulloides* (Gb) picked from the >150 μm size fraction. Radiocarbon samples were analysed at the Keck AMS facility at U.C. Irvine. Radiocarbon dates were calibrated with Calib 7.0 using the Marine13 calibration curve and a marine reservoir correction of 850 ± 100 yr. The 2-σ midpoint age, rounded to the nearest decade, is used for the age model. One sample was excluded from the age model due to a minor age reversal (denoted with an asterisk), although this date is within uncertainty of the adjacent shallower radiocarbon date, indicating very high sedimentation rates in this section of the core.